Applied Physics Letters ARTICLE scitation.org/journal/apl

An efficient method to boost the short-circuit current of quantum-dot-sensitized solar cells

Cite as: Appl. Phys. Lett. **114**, 043901 (2019); doi: 10.1063/1.5082575
Submitted: 21 November 2018 · Accepted: 14 January 2019 · Published Online: 30 January 2019

Shaokang Dong, Shengjun Li,[a] Junhao Cai, Zeng Chen, Chaochao Wei, Xijin Li, Yaru Peng, Furui Tan,[a] and Weifeng Zhang

AFFILIATIONS

Henan Key Laboratory of Photovoltaic Materials, Henan University, Kaifeng 475001, China

[a] **Authors to whom correspondence should be addressed**: Lishengjun1011@126.com and frtan2012@163.com.
Tel./Fax: 86-378-3881602

ABSTRACT

According to the Marcus theory, the driving force for the transfer of photogenerated electrons from quantum dots (QDs) to oxide nanocrystals depends on the energy difference of the system. In this study, an efficient driving force for the transfer of photoinduced charge–inner electric field effects–was suggested. The inner electric field was introduced from the p-NiO/n-ZnO heterojunction, which was formed by the *in situ* deposition of NiO on the ZnO nanosheet/nanorod film surface. Photoluminescence spectra revealed that the photogenerated charge carriers can be efficiently separated at the interface of p-NiO/n-ZnO. The QD-sensitized solar cells (QDSCs) assembled with the p-NiO/n-ZnO photoanodes exhibited considerably higher J_{SC} compared to those fabricated with ZnO photoanodes, indicating that the formation of a p–n junction at the photoanode surface is an efficient strategy to boost the short-circuit current of QDSCs.

Quantum-dot-sensitized solar cells (QDSCs) have attracted increasing attention due to their potential to replace the currently used conventional solar cells.[1–3] In the past few years, the power conversion efficiency (PCE) of QDSCs has been improved to greater than 12%, which is comparable to that of other solar cells.[4,5] Meanwhile, QDSCs exhibit other advantages, including a high theoretical PCE; simple preparation; and low cost. QDSCs mainly comprise three components, i.e., a photoanode, a polysulfide electrolyte, and a counter electrode (CE). The photoanode is a QD-sensitized metal oxide, which is responsible for the efficient separation of photogenerated charges and the collection of electrons. The properties of photoanodes are key for improving short-circuit current densities of QDSCs. Several techniques for improving the photoanodes to achieve a high short-circuit current density are available. The first strategy includes the optimization of QD sensitizers, such as the selection of QDs; the design of the QD structure; and the deposition route of QDs.[6–11] The second strategy includes the modification of metal oxide, such as the use of one-dimensional- and hierarchical-structured films; the coating of wide-band-gap materials; and organic molecular treatment.[12–16]

According to the Marcus theory, the dynamics of the photoinduced charge transfer from the QD to the oxide depends on the driving force (the energy difference between the donor and acceptor levels) as well as on the donor–acceptor electronic coupling strength.[17,18] In this paper, NiO was deposited *in situ* on the ZnO nanosheet/nanorod film surface, affording a p–n junction. When a p–n heterojunction was formed by p-type NiO and n-type ZnO, the hole and the electron at the p-NiO/n-ZnO interface are transferred in a certain direction by the concentration difference as the driving force. Hence, an inner electric field is formed at the interface. This internal electric field of the formed p–n junction is designed to supply another driving force for the transfer of the photoinduced charge.

In our previously reported studies, a hierarchical ZnO-nanosheet-nanorod-structured film was obtained, which could be used as an efficient substrate material for the photoanode in QDSCs.[19] In addition, the hierarchical ZnO NS–NR film was used in this experiment. Figure 1 shows the morphologies of the ZnO NS–NR film after different treatment times in the $NiCl_2$ solution. The morphology of the ZnO NS–NR film exhibited almost no changes, with the exception that the edge of the ZnO nanorod

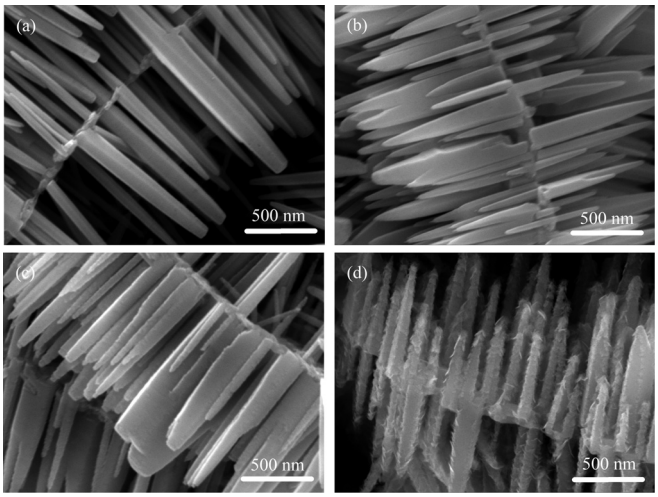

FIG. 1. FE-SEM micrographs of the p-NiO/n-ZnO film prepared by treatment in $NiCl_2$ solution at different periods of time: (a) 30 s, (b) 1 min, (c) 4 min, and (d) 8 min.

became blunt at a treatment time of 30 s. The following reactions possibly occurred on the ZnO film surface.

$$NiCl_2 + H_2O \rightarrow Ni(OH)_2 + 2H^+ + 2Cl^-,$$
$$ZnO + 2H^+ \rightarrow Zn^{2+} + H_2O.$$

ZnO was dissolved in the solution by the deposition of $Ni(OH)_2$, especially the edge and termini of the ZnO nanorod. The deposited $Ni(OH)_2$ was sintered to NiO. After 1-min treatment in the $NiCl_2$ solution, the ZnO nanorod was more cuspidal, and the edge became more blunt than that obtained after 30-s treatment. The ZnO nanorod surface became rough with the extension of the treatment time to 4 min. At a treatment time of 8 min, some nanoplate-structured NiO was observed. NiO-layers were well distributed on the ZnO film surface.

TEM images were recorded to further investigate the p-NiO/n-ZnO interface. The sample was the ZnO film after 1-min treatment in the $NiCl_2$ solution. The p-NiO/n-ZnO composite film was scraped from the FTO substrate and dispersed in ethanol. Figure 2(a) shows the TEM image of one NiO-coated ZnO nanorod. A 2–5-nm thin film was present outside the ZnO nanorod, which should be NiO according to the preparation. The Energy Dispersive Spectrometer (EDS) spectral (Fig. S2) results revealed that the Ni content is ~1.31% (at. %). Figure 2(b) shows the high-resolution TEM image of p-NiO/n-ZnO. Regular crystal lattice lines of ZnO were observed, and the spacing between the adjacent lattice fringes was ~0.265 nm, corresponding to the interplanar distance of the (002) crystal planes in wurtzite ZnO. However, the crystal lattice lines were extremely fuzzy, corresponding to the NiO layer outside the ZnO nanorod.

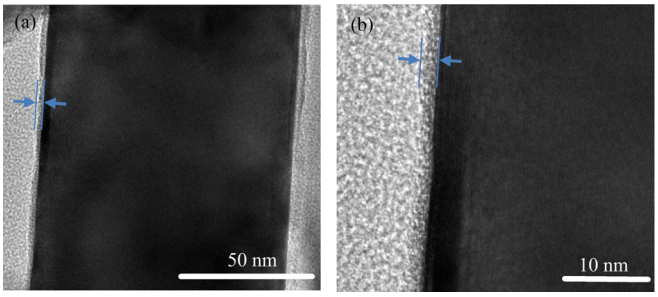

FIG. 2. (a) Low-magnification and (b) high-magnification TEM images of the p-NiO/n-ZnO film prepared by 1-min treatment in the $NiCl_2$ solution.

To confirm the formation of the p-NiO/n-ZnO heterojunction, the electrical properties of ZnO, NiO, and p-NiO/n-ZnO films were investigated through current-voltage measurements under dark DC bias conditions. The I–V and semi-log current-voltage curves are shown in Figs. 3(a) and 3(b). The schematic diagram of the I–V testing system is illustrated in the inset of Fig. 3(a). Both In/n-ZnO/Au and In/p-NiO/Au structures exhibited ohmic behaviors. Figure 3(b) shows the direct difference among In/n-ZnO/Au, In/p-NiO/Au, and In/n-ZnO/p-NiO/Au structures. The sections of log I–V in reverse bias of both In/n-ZnO/Au and In/p-NiO/Au structures looked almost as mirror images of those obtained in forward bias. However, the In/n-ZnO/p-NiO/Au structure depicted nonlinear I–V curves and obvious rectifying behavior, indicating the formation of the p-n heterojunction at the NiO and ZnO layer interface. The threshold voltage for the as-prepared p-NiO/n-ZnO heterojunction was estimated to be about 0.9 V, and leakage current under the reverse bias of −2.0 V was 0.0382 mA. Hence, the threshold voltage was much lower than the reported values of p-NiO/n-ZnO heterojunctions.[20,21] This phenomenon might be related to the thickness of the NiO layer at ZnO substrate surfaces.[21] The ratio between I_F (current under the forward bias of 2 V) and I_R (current under the reverse bias of −2 V) for the In/n-ZnO/p-NiO/Au structure was estimated to be 133, suggesting the formation of the high-quality p-n heterojunction.

Figure 4(a) shows the PL spectra of ZnO and the p-NiO/n-ZnO film. The p-NiO/n-ZnO film exhibited a considerably lower emission intensity compared to the ZnO film, indicating that the photogenerated charge carriers can be efficiently separated at the p-NiO/n-ZnO interface. The recombination of the separated electrons and holes was considerably restrained. Figure 4(b) shows the normalized PL spectra of the ZnO and NiO/ZnO film. The visible emission of the p-NiO/n-ZnO film was not enhanced in comparison with that of the ZnO film, indicating that the NiO coating should not introduce an additional oxygen vacancy on the ZnO film surface.[23,24] Generally, the growth of the NiO layer did

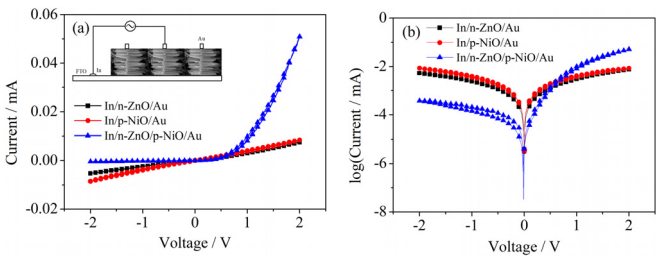

FIG. 3. *I-V* (a) and semi-log *I-V* (b) curves of ZnO, NiO, and p-NiO/n-ZnO films.

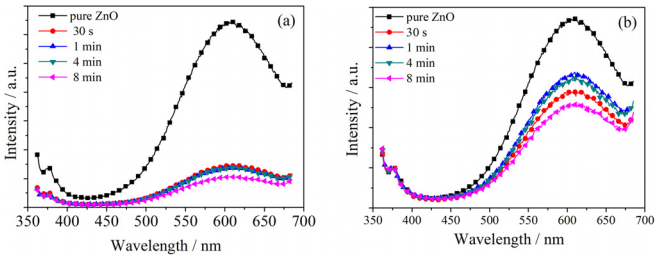

FIG. 4. PL emission spectra (a) and normalized PL spectra (b) of the p-NiO/n-ZnO film prepared by treatment in the $NiCl_2$ solution for different times.

not destroy the ZnO lattice, and the photogenerated charge carriers were smoothly transferred to the p-NiO/n-ZnO interface.

The obtained p-NiO/n-ZnO films were sensitized with CdS and CdSe QDs, which were then assembled with the PbS counter electrode for preparing QDSCs.[22,25] The photoelectric conversion efficiencies of QDSCs based on the p-NiO/n-ZnO photoanodes were estimated under the illumination of an AM 1.5 G solar simulator with an intensity of 100 mW cm^{-2}. More than five cells were tested for each sample prepared at a certain treating time in NiO sol-gel. Figure 5(a) shows the J–V curves. Table I shows the photovoltaic parameters of the QDSCs. The fill factor (FF) decreased from 0.49 to 0.43 after 30 s treatment in NiO sol–gel. The FF value then gradually increased to 0.52 with extension of treatment time, consistent with changes in dark current (Fig. S3). The dark current showed significant enhancement using the treatment time of 30 s. The dark current successively weakened as the treatment time rose from 30 s to 8 min. However, the open-circuit voltage (V_{OC}) did not exhibit the same changing trends with FF and dark current. V_{OC} illustrated obvious enhancement after 1 min treatment in NiO sol–gel, which might be related to changes in electron density of the photoanode.[26] The increase in the carrier concentration might cause the reduction of the entropy production per photon and consequently enhances the open circuit voltage. Meanwhile, V_{OC} displayed a sharp decline at treatment times longer than 4 min. Electrochemical impedance spectroscopy (EIS) was carried out to investigate the reasons behind the changes in V_{OC} (Fig. S4). The electron effective lifetimes (τ_e) were also obtained from EIS. τ_e of the ZnO photoanode shortened from 54.0 to 19.6 ms after 30s treatment in NiO sol–gel. τ_e exhibited few changes using longer treatment times than 1 min. Hence, τ_e

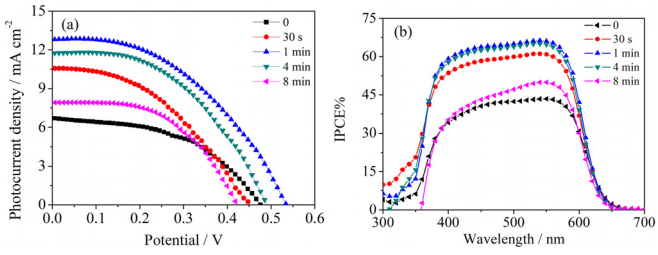

FIG. 5. Photocurrent density–voltage (a) and IPCE (b) curves of QDSCs using CdS–CdSe quantum-dot-sensitized p-NiO/n-ZnO films as photoanodes.

TABLE I. Photovoltaic characteristics of the QDSCs using CdS–CdSe quantum-dot-sensitized p-NiO/n-ZnO films as photoanodes.

Treatment time	J_{SC}/mA cm^{-2}	V_{OC}/mV	*FF*	*PCE*/%
0	6.70	481	0.49	1.58
30 s	10.57	447	0.43	2.03
1 min	12.82	540	0.45	3.08
4 min	11.76	492	0.48	2.75
8 min	7.92	424	0.52	1.76

should not be the main reason behind changes in V_{OC}, which requires further future investigations.

Different from V_{OC} and FF, the short-circuit current (J_{SC}) sharply increased from 6.70 mA cm^{-2} to 12.82 mA cm^{-2} after 1-min treatment in the $NiCl_2$ solution. However, J_{SC} significantly decreased with further extension of the treatment time. In addition, the changes of J_{SC} were observed in the IPCE spectra [Fig. 5(b)]. The Monochromatic Incident Photon-to-Electron Conversion Efficiency (IPCE) value significantly improved in the entire light absorption range of 350 nm to 650 nm at a treatment time of 1 min. At a treatment time of 8 min, the IPCE value was even less than that of the pure ZnO photoanode, except in the long wavelength range (500–600 nm). The changes of J_{SC} were possibly related to the formation of a NiO layer on the ZnO surface. Under the illumination of a solar simulator, the electrons in the valence band of CdS and CdSe QDs are possibly excited and transferred to the conduction band under the driving force of the energy difference between QDs and ZnO levels. In the p-NiO/n-ZnO photoanodes, a p–n heterojunction was formed at the interface between p-NiO and n-ZnO (Fig. 6). The inner electric field of this p–n heterojunction might supply a driving force for the transfer of photoelectrons. On the other hand, the transfers of charge carriers between CdS (or CdSe) QDs and NiO films have been verified previously.[27] When the photoelectrons were transferred into the inner electric field of p-NiO/n-ZnO, the transfer rate of electrons will be accelerated by the electric field force. Hence, J_{SC} is sharply improved. However, with an extremely thick NiO, the photoelectrons from the CdS (or CdSe) QDs were not directly transferred into the inner electric field of p-NiO/n-ZnO. The photoelectrons had to

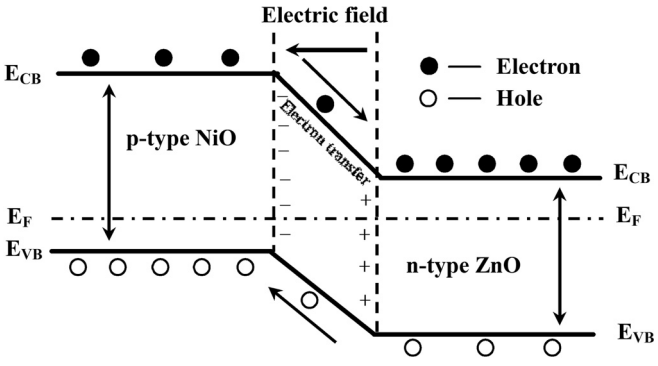

FIG. 6. Schematic of the p-NiO/n-ZnO film band structure.

pass through the excess NiO layer before arriving at the inner electric field, which would delay the transfer rate of electrons; hence, J_{SC} significantly decreases.

A uniform NiO layer was deposited on the ZnO NS–NR-structured film surface to form a p-NiO/n-ZnO heterojunction. FESEM, EDS, and TEM results confirmed the formation of the NiO layer. PL spectra revealed that the photogenerated charge carriers can be efficiently separated at the p-NiO/n-ZnO interface. The p-NiO/n-ZnO photoanodes exhibited considerably higher J_{SC} compared to the ZnO photoanodes when these films were assembled into QDSCs. J_{SC} probably improved owing to the introduction of an efficient driving force for the photoelectron transfer processes—the inner electric field effects.

See supplementary material for the details on the preparation of p-NiO/n-ZnO photoanodes, assembling of QDSCs, and measurement conditions.

This work was financially supported by the Natural Science Foundation of China (Nos. U1404202 and 21403056), Program for Science and Technology Innovation Talents in Universities of Henan Province (18HASTIT031), and the Key Science and Technology Project of Henan Province (182102210243).

REFERENCES

[1]P. V. Kamat, J. Phys. Chem. C **112**, 18737 (2008).
[2]Y. L. Lee and Y. S. Lo, Adv. Funct. Mater. **19**, 604 (2009).
[3]P. K. Santra and P. V. Kamat, J. Am. Chem. Soc. **134**, 2508 (2012).
[4]S. Jiao, J. Du, Z. Du, D. Long, W. Jiang, Z. Pan, Y. Li, and X. Zhong, J. Phys. Chem. Lett. **8**, 559 (2017).
[5]W. Wang, W. Feng, J. Du, W. Xue, L. Zhang, L. Zhao, Y. Li, and X. Zhong, Adv. Mater. **30**, 1705746 (2018).
[6]N. T. Thao, H. N. Phuong, H. T. Tung, N. T. Phat, H. T. Dat, and L. Q. Vinh, Opt. Mater. **84**, 199 (2018).
[7]S. S. Lo, T. Mirkovic, C. H. Chuang, C. Burda, and G. D. Scholes, Adv. Mater. **23**, 180 (2011).
[8]D. Ghosh, A. Ghosh, M. Y. Ali, and S. Bhattacharyya, Chem. Mater. **30**, 6071 (2018).
[9]M. A. Abate and J. Y. Chang, Sol. Energy Mater. Sol. Cells **182**, 37 (2018).
[10]G. Halder and S. Bhattacharyya, J. Mater. Chem. A **5**, 11746 (2017).
[11]J. Hou, H. F. Zhao, F. Huang, L. Chen, Q. Wu, Z. Y. Liu, S. L. Peng, N. Wang, and G. Z. Cao, J. Mater. Chem. A **6**, 9866 (2018).
[12]H. N. Chen, L. Q. Zhu, H. C. Liu, and W. P. Li, Nanotechnology **23**, 075402 (2012).
[13]J. J. Tian, E. Uchaker, Q. F. Zhang, and G. Z. Cao, ACS Appl. Mater. Interfaces **6**, 4466 (2014).
[14]Y. F. Xu, W. Y. Chen, X. H. Ding, X. Pan, L. H. Hu, S. F. Yang, J. Zhu, and S. Y. Dai, Inorg. Chem. Front. **5**, 1370 (2018).
[15]M. Raissi, M. T. Sajjad, Y. Farre, T. J. Roland, A. Ruseckas, I. D. W. Samuel, and F. Odobel, Sol. Energy Mater. Sol. Cells **181**, 71 (2018).
[16]K. Zhao, Z. X. Pan, I. Mora-Seró, E. Cańovas, H. Wang, Y. Song, X. Gong, J. Wang, M. Bonn, J. Bisquert, and X. Zhong, J. Am. Chem. Soc. **137**, 5602 (2015).
[17]S. Y. Jin and T. Q. Lian, Nano Lett. **9**, 2448 (2009).
[18]K. Tvrdy, P. A. Frantsuzov, and P. V. Kamata, PNAS **108**, 29 (2011).
[19]J. H. Cai, Z. Chen, S. J. Li, S. K. Dong, C. C. Wei, F. M. Li, Y. R. Peng, X. Y. Jia, and W. F. Zhang, Electrochim. Acta **274**, 326 (2018).
[20]A. Echresh, M. A. Abbasi, M. Z. Shoushtari, M. Farbod, O. Nur, and M. Willander, Semicond. Sci. Technol. **29**, 115009 (2014).
[21]B. O. Jung, Y. H. Kwon, D. J. Seo, D. S. Lee, and H. K. Cho, Cryst. Growth **370**, 314 (2013).
[22]Z. Chen, C. C. Wei, S. J. Li, C. L. Diao, W. Li, W. P. Kong, Z. L. Zhang, and W. F. Zhang, Nanoscale Res. Lett. **11**, 295 (2016).
[23]Z. Y. Zhang, C. L. Shao, X. H. Li, C. H. Wang, M. Y. Zhang, and Y. C. Liu, ACS Appl. Mater. Interfaces **2**, 2915 (2010).
[24]Y. H. Zheng, C. Q. Chen, Y. Y. Zhan, X. Y. Lin, Q. Zheng, K. M. Wei, and J. F. Zhu, J. Phys. Chem. C **112**, 10773 (2008).
[25]Q. Q. Pei, Z. Chen, S. Wang, D. Zhang, P. Ma, S. J. Li, X. W. Zhou, and Y. Lin, Sol. Energy **178**, 108 (2019).
[26]R. Brendel and H. J. Queisser, Sol. Energy Mater. Sol. Cells **29**, 397 (1993).
[27]W. P. Kong, S. J. Li, Z. Chen, C. C. Wei, W. Li, T. Li, Y. Yan, X. Y. Jia, B. H. Xu, and W. F. Zhang, Part. Part. Syst. Charact. **32**, 1078 (2015).